DINAME 2017 - Proceedings of the XVII International Symposium on Dynamic Problems of Mechanics
A. T. Fleury, D. A. Rade, P. R. G. Kurka (Editors), ABCM, São Sebastião, SP, Brazil, March 5-10, 2017

Yaw stability analysis of articulated vehicles using phase trajectory method

André de Souza Mendes[1,2], **Marko Ackermann**[1], **Fabrizio Leonardi**[1], **Agenor de Toledo Fleury**[1,2]

[1] Centro Universitário FEI. Av. Humberto de Alencar Castelo Branco, 3972 - Assunção, São Bernardo do Campo - SP, asmendes@fei.edu.br, mackermann@fei.edu.br, fabrizio@fei.edu.br, agfleury@fei.edu.br

[2] Escola Politécnica da USP. Cidade Universitária, São Paulo - SP

Abstract: This paper addresses the yaw stability analysis of articulated vehicles using the phase trajectory method. The goal of this work is to ascertain the dynamic conditions that the articulated vehicle can assume without the occurrence of instability events such as jackknife and rollover. The study focuses on the vehicle configuration composed by one tractor unit and a driven unit such as, for instance, a tractor semi-trailer combination. The system consists of a nonlinear tire model and a nonlinear articulated bicycle model with four degrees of freedom. The analysis presented in this paper illustrates the convergence regions of equilibrium points obtained through numerical integration of the equations of motion of the model for different initial conditions in the phase plane. In addition, the changes in the obtained regions are presented as a function of the tractor speed and the position of the articulation point between the two units.

Keywords: Vehicle dynamics, Articulated vehicles, Stability analysis, Phase trajectory method, Jackknife

NOMENCLATURE

Latin symbols

a: tire parameters
a, b, c, d, e: vehicle distances
B: stiffness factor
C: shape factor
D: peak factor
E: curvature factor
F, T, R, A, S, M: vehicle points
F: Force
I: moment of inertia
m: mass
M, f: matrix elements
$\mathbf{M}$, $\mathbf{f}$: vector functions
n: tire number
$\mathbf{t}$, $\mathbf{s}$, $\mathbf{e}$: versors
$\mathbf{u}$: input vector
$\mathbf{v}$: velocity vector
v: vehicle speed
$\mathbf{x}$: state vector
x: state variable
x, y: position coordinates
w: width

Greek symbols

α, β: slip angle
δ: steering angle
ϕ: articulation angle
γ: camber angle
μ: friction coefficient
Ω: base
ψ: yaw angle

Subscripts

eq: equivalent
F, T, R, A, S, M: vehicle points
f: final
n: nominal
S: semitrailer
T: tractor
x: longitudinal
y: transversal
z: vertical

INTRODUCTION

In heavy weight truck operations, driver and fuel are significant sources of spending. So, in economic terms, the owners seek to transport the maximum amount of cargo with the lowest possible vehicle weight (Fancher and Winkler, 2007). However, the increase of load capacity implies, in most cases, in the increase of vehicle dimensions which are limited by legislation and structural characteristics of the roads. Very long vehicles are not able to perform tight turns because the rearmost axle tends to move towards the lateral limits of the road not following the path imposed by the front axle. This phenomenon is called offtracking (Ejzenberg, 2009). By splitting long vehicles into several units with shorter wheelbase distances and connecting them through articulations, a higher level of maneuverability can be achieved and tight curves can be made. However, with this vehicle configuration, instability events such as jackknife may occur.

To better understand the yaw instability events associated with articulated vehicles, this paper aims to verify in which dynamic conditions the system, without any input (steering angle, breaking and acceleration), returns to travel in a straight line without the occurrence of any instability phenomenon. Based on this information it is possible to obtain a region in the phase plane that gathers the set of dynamic conditions that satisfy this requirement. Furthermore, the influence of some parameters on the shape of this region should be checked, such as the speed of the tractor and the position of the articulation point.

STABILITY ANALYSIS OF ARTICULATED VEHICLES

Relatively recent studies present yaw stability analysis of articulated vehicles using linear models (Maas, 2007) (Hac, Fulk and Chen, 2008) (Luijten, 2010). The applicability of such models is studied by Islam *et al.* (2014). The authors verify different linear models of articulated vehicles to be used in stability and dynamic simulation analysis. Dynamic results from single lane changes are compared to those from a nonlinear experimentally validated model developed in the software *TruckSim*. Good agreement was obtained between the linear and nonlinear models for maneuvers with low overall lateral acceleration ($0.3\,g$). When the lateral acceleration exceeds $0.3\,g$ the linear models begin to present significant errors, showing their limitations in reproducing reality. Furthermore, the nonlinear relationship between the lateral force and the slip angle, also known as tire characteristic curve, has a great influence on the dynamic behavior of vehicles (Ervin *et al.*, 1979). This relationship interferes directly in the stability boundaries of vehicles and its shape depends primarily on the friction coefficient, the vertical load and the longitudinal force of the tire (Pacejka, 2006). In an effort to take into consideration the nonlinear behavior of the characteristic curve, many authors use a third order polynomial model (Johnson and Huston, 1984) (Samsundar and Huston, 1998) (Sadri and Wu, 2013). An alternative for purely numerical simulation is the semi-empirical model known as *Magic Formula* (Pacejka, 2006) which is also widely used (Stotsky and Hu, 1997) (Pauwelussen, 2001) (Wideberg, Dahlberg and Svensson, 2009).

The stability analysis of nonlinear systems, if not linearized, can be performed using the Lyapunov direct method and the phase trajectories method. The first consists in determining stability based on a fictitious energy function called Lyapunov function. Applications of this method in vehicle systems can be found in Yin *et al.* (2015) and Yan, Xu and Liu (2015). The second method is based on the analysis of the behavior of the orbits of the model states from different initial conditions. Ding *et al.* (2014) use the phase trajectories method to determine the stability regions of a nonlinear model of a tractor-semitrailer combination. Moreover, the authors analyze the variation of the stability region by changing vehicle parameters such as speed and friction coefficient value. However, the model used, although not linear, assumes that the longitudinal speed of the tractor and that of the trailer are equal and constant, which can lead to anomalous results for conditions distant from the equilibrium points. Sun and He (2015) use the phase plane to check the stability of nonlinear articulated vehicle model in single lane change maneuvers with open loop sinusoidal steering input. The trajectories of the state variables are compared to the dynamic behavior of a 21 DOF *CarSim* model. Thus, the authors determine the maximum steering value allowed in this maneuver without the occurrence of instability events.

It is possible to notice that there is a trend in the use of nonlinear models of articulated vehicles in stability analysis because, in certain scenarios, linear models are not able to reproduce the vehicle behavior with the necessary accuracy. Moreover, the importance of using an appropriate method for identifying the equilibrium points and regions of stability is evident. A more comprehensive discussion on the present topic can be found in Mendes (2016).

MATHEMATICAL MODELS

The mathematical model of the tractor-semitrailer combination for yaw stability analysis must be able to represent the dynamic behavior, at least qualitatively, of an actual vehicle for the entire phase plane domain. However, for high values of friction coefficient and high lateral acceleration yaw instability may not occur, resulting instead in rollover event (Ding *et al.*, 2014). This type of instability occurs when the lateral acceleration exceeds a certain value, known as rollover threshold (Winkler and Ervin, 1999). The typical value of this lateral acceleration limit is between 0.2 and $0.5\,g$ for articulated trucks. In contrast, if the friction coefficient is low it is possible to reach the nonlinear region of the tire characteristic curve even under low lateral acceleration. Therefore, for maneuvers at high speed and low friction coefficient the risk of jackknife exists and involves the nonlinear characteristics of the tires. Thus, the chosen tire model is based on the *magic formula* tire model, because it is able to adequately represent the tire lateral force for the entire range of slip angles. Furthermore, the vehicle model is a nonlinear bycicle model with 4 DOF and do not take into consideration the roll dynamics. In this case, the rollover threshold is used to determine the occurance of rollover event. Both models are detailed as follows.

Magic formula tire model

The nonlinear tire model is a simplified version of the *magic formula* tire model (Bakker, Pacejka and Lidner, 1989). The tire lateral force can be written as

$$F_y = \frac{\mu}{\mu_n} F_{y,n}(\alpha_{eq}), \tag{1}$$

where μ and μ_n are the operational and nominal friction coefficients, respectively. The nominal function $F_{y,n}$ is given by

$$F_{y,n} = D\sin\left[C\arctan B\alpha - E(B\alpha - \arctan(B\alpha))\right] \tag{2}$$

and the equivalent slip angle α_{eq} is calculated as

$$\alpha_{eq} = \frac{\mu_n}{\mu}\alpha, \tag{3}$$

where α is the actual tire slip angle.

The stiffness factor B, the shape factor C, the peak factor D and the curvature factor E from Eq. 2 are calculated as

$$B = \frac{1}{CD}\mathtt{a}_3 \sin\left\{2\arctan\left(\frac{F_z}{\mathtt{a}_4}\right)\right\}(1-\mathtt{a}_5|\gamma|) \tag{4}$$

$$C = \mathtt{a}_0 \tag{5}$$

$$D = \mu F_z = (\mathtt{a}_1 F_z + \mathtt{a}_2) F_z \tag{6}$$

$$E = \mathtt{a}_6 F_z + \mathtt{a}_7, \tag{7}$$

where F_z is the vertical load, γ is the camber angle and the parameters $\mathtt{a}_0$, $\mathtt{a}_1$, $\mathtt{a}_2$, $\mathtt{a}_3$, $\mathtt{a}_4$, $\mathtt{a}_5$, $\mathtt{a}_6$ and $\mathtt{a}_7$ are responsible for fitting the tire model according to the experimental tire curve.

Articulated vehicle model

The physical model of the vehicle combination is shown in Fig. 1. To characterize the dynamics of this system the vector base $\Omega_O = \{O\mathbf{ijk}\}$ fixed to the inertial reference frame is used. The moving vector base $\Omega_T = \{T\mathbf{t}_x\mathbf{t}_y\mathbf{t}_z\}$ is fixed to the tractor and the vector base $\Omega_S = \{S\mathbf{s}_x\mathbf{s}_y\mathbf{s}_z\}$ is fixed to the semitrailer. The base $\Omega_F = \{F\mathbf{e}_x\mathbf{e}_y\mathbf{e}_z\}$ is fixed to the front axle to assist the description of the steering and slip angles. The points T and S locate the center of gravity (CG) of the tractor and semitrailer, respectively. F, R and M locate the axles of the vehicle and A is the articulation point. The distances a, b and c separate the points F, T, R and A of the tractor and the distances d and e separates the points A, S and M of the semitrailer. The velocity vectors $\mathbf{v}$ and slip angles α receive the subscripts regarding the points to which they are associated.

The modeling of the tractor-semitrailer combination is done considering two rigid bodies moving on a horizontal plane and joined by a single articulation point. Thus, the model has four degrees of freedom. The generalized coordinates can be given by x, y, ψ and ϕ. x and y are the coordinates of the center of gravity of the tractor. ψ is the yaw angle of the tractor and ϕ is the relative yaw angle of the semitrailer. The equations of motion were developed using the Lagrangian approach.

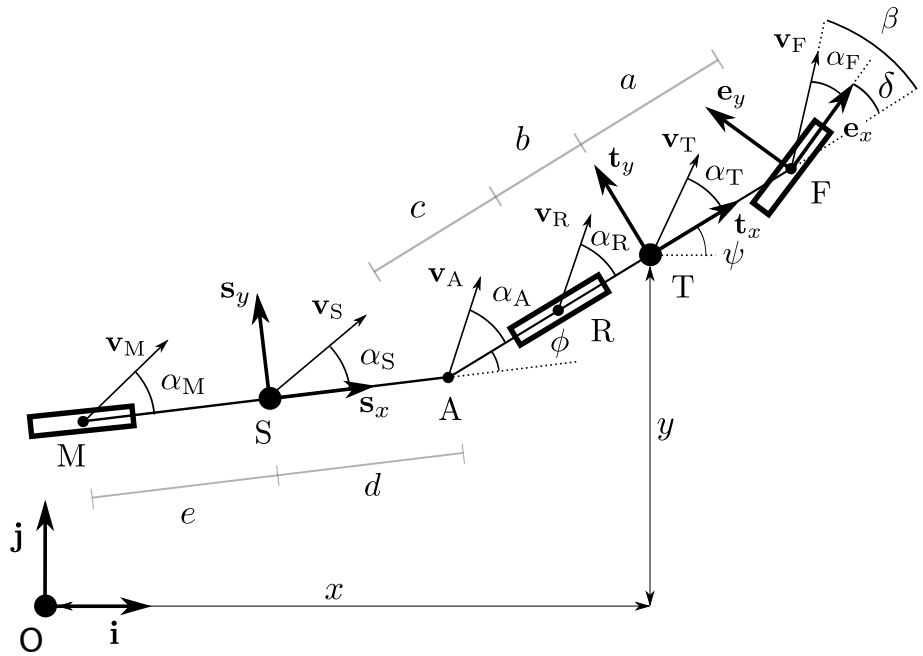

Figure 1 – Single track bicycle model.

The nonlinear system state equation can be written as

$$\mathbf{M}(\mathbf{x})\dot{\mathbf{x}} = \mathbf{f}(\mathbf{x},\mathbf{u}), \tag{8}$$

where the state vector is

$$\mathbf{x} = \begin{bmatrix} \mathrm{x}_1 & \mathrm{x}_2 & \mathrm{x}_3 & \mathrm{x}_4 & \mathrm{x}_5 & \mathrm{x}_6 & \mathrm{x}_7 & \mathrm{x}_8 \end{bmatrix}^T = \begin{bmatrix} x & y & \psi & \phi & v_\mathrm{T} & \alpha_\mathrm{T} & \dot{\psi} & \dot{\phi} \end{bmatrix}^T \tag{9}$$

and the input vector is

$$\mathbf{u} = \begin{bmatrix} \delta & F_{x,\mathrm{F}} & F_{x,\mathrm{R}} & F_{x,\mathrm{M}} \end{bmatrix}^T. \tag{10}$$

where δ is the steering angle and $F_{x,\mathrm{F}}$, $F_{x,\mathrm{R}}$ and $F_{x,\mathrm{M}}$ are the longitudinal forces at each axle.

The matrix $\mathbf{M}$ is

$$\mathbf{M} = \begin{bmatrix} 1 & 0 & 0 & 0 & 0 & 0 & 0 & 0 \\ 0 & 1 & 0 & 0 & 0 & 0 & 0 & 0 \\ 0 & 0 & 1 & 0 & 0 & 0 & 0 & 0 \\ 0 & 0 & 0 & 1 & 0 & 0 & 0 & 0 \\ 0 & 0 & 0 & 0 & M_{55} & M_{56} & M_{57} & M_{58} \\ 0 & 0 & 0 & 0 & M_{65} & M_{66} & M_{67} & M_{68} \\ 0 & 0 & 0 & 0 & M_{75} & M_{76} & M_{77} & M_{78} \\ 0 & 0 & 0 & 0 & M_{85} & M_{86} & M_{87} & M_{88} \end{bmatrix}, \tag{11}$$

where the elements are given as

$$M_{55} = (m_T + m_S)\cos(\psi + \alpha_{\mathrm{T}}) \tag{12}$$
$$M_{56} = -(m_T + m_S)\, v_{\mathrm{T}} \sin(\psi + \alpha_{\mathrm{T}}) \tag{13}$$
$$M_{57} = m_S[(b+c)\sin\psi + d\sin(\psi - \phi)] \tag{14}$$
$$M_{58} = -m_S d \sin(\psi - \phi) \tag{15}$$
$$M_{65} = (m_T + m_S)\sin(\psi + \alpha_{\mathrm{T}}) \tag{16}$$
$$M_{66} = (m_T + m_S)\, v_{\mathrm{T}} \cos(\psi + \alpha_{\mathrm{T}}) \tag{17}$$
$$M_{67} = -m_S[(b+c)\cos\psi + d\cos(\psi - \phi)] \tag{18}$$
$$M_{68} = m_S d \cos(\psi - \phi) \tag{19}$$
$$M_{75} = -m_S[(b+c)\sin\alpha_{\mathrm{T}} + d\sin(\alpha_{\mathrm{T}} + \phi)] \tag{20}$$
$$M_{76} = -m_S[(b+c)\, v_{\mathrm{T}} \cos\alpha_{\mathrm{T}} + d v_{\mathrm{T}} \cos(\alpha_{\mathrm{T}} + \phi)] \tag{21}$$
$$M_{77} = m_S[(b+c)^2 + 2(b+c)\, d\cos\phi + d^2] + I_T + I_S \tag{22}$$
$$M_{78} = -m_S[(b+c)\, d\cos\phi + d^2] + I_S \tag{23}$$
$$M_{85} = m_S d \sin(\alpha_{\mathrm{T}} + \phi) \tag{24}$$
$$M_{86} = m_S d v_{\mathrm{T}} \cos(\alpha_{\mathrm{T}} + \phi) \tag{25}$$
$$M_{87} = -m_S[d^2 + (b+c)\, d\cos\phi] + I_S \tag{26}$$
$$M_{88} = \left(m_S d^2 + I_S\right). \tag{27}$$

The vector function $\mathbf{f}$ is given as

$$\mathbf{f} = \begin{bmatrix} v_{\mathrm{T}}\cos(\psi + \alpha_{\mathrm{T}}) & v_{\mathrm{T}}\sin(\psi + \alpha_{\mathrm{T}}) & \dot{\psi} & \dot{\phi} & f_5 & f_6 & f_7 & f_8 \end{bmatrix}^T, \tag{28}$$

where

$$\begin{aligned} f_5 &= F_{x,\mathrm{F}}\cos(\psi + \delta) + F_{x,\mathrm{R}}\cos\psi + F_{x,\mathrm{M}}\cos(\psi - \phi) - F_{y,\mathrm{F}}\sin(\psi + \delta) - F_{y,\mathrm{R}}\sin\psi - F_{y,\mathrm{M}}\sin(\psi - \phi) - \ldots \\ \ldots &- m_S(b+c)\,\dot{\psi}^2\cos\psi - m_S d\left(\dot{\psi} - \dot{\phi}\right)^2\cos(\psi - \phi) + (m_T + m_S)\, v_{\mathrm{T}}\sin(\psi + \alpha_{\mathrm{T}})\,\dot{\psi} \end{aligned} \tag{29}$$

$$\begin{aligned} f_6 &= F_{x,\mathrm{F}}\sin(\psi + \delta) + F_{x,\mathrm{R}}\sin\psi + F_{x,\mathrm{M}}\sin(\psi - \phi) + F_{y,\mathrm{F}}\cos(\psi + \delta) + F_{y,\mathrm{R}}\cos\psi + F_{y,\mathrm{M}}\cos(\psi - \phi)\ldots \\ \ldots &- m_S(b+c)\,\dot{\psi}^2\sin\psi - m_S d\left(\dot{\psi} - \dot{\phi}\right)^2\sin(\psi - \phi) - (m_T + m_S)\, v_{\mathrm{T}}\cos(\psi + \alpha_{\mathrm{T}})\,\dot{\psi} \end{aligned} \tag{30}$$

$$\begin{aligned} f_7 &= F_{x,\mathrm{F}} a\sin\delta + F_{x,\mathrm{M}}(b+c)\sin\phi + F_{y,\mathrm{F}} a\cos\delta - F_{y,\mathrm{R}} b - F_{y,\mathrm{M}}[(b+c)\cos\phi + (d+e)] - \ldots \\ \ldots &- m_S(b+c)\, d\left(\dot{\psi} - \dot{\phi}\right)^2\sin\phi + m_S(b+c)\, d\dot{\psi}^2\sin\phi + m_S[(b+c)\, v_{\mathrm{T}}\cos\alpha_{\mathrm{T}} + d v_{\mathrm{T}}\cos(\alpha_{\mathrm{T}} + \phi)]\,\dot{\psi} \end{aligned} \tag{31}$$

$$f_8 = F_{y,\mathrm{M}}(d+e) - m_S(b+c)\, d\dot{\psi}^2\sin\phi - m_S d v_{\mathrm{T}}\cos(\alpha_{\mathrm{T}} + \phi)\,\dot{\psi}. \tag{32}$$

SIMULATION MODEL

The mathematical models described above are implemented in a open source simulation package called *Vehicle Dynamics - Lateral* (Mendes and Meneghetti, 2015). This package is written in *Matlab* through an object-oriented programming architecture and contains the necessary properties and functions to simulate and analyze the yaw dynamic

Table 1 – Articulated vehicle model - Vehicle parameters.

Item	Description	Value	Unit
m_{T}	Mass of the tractor	$7,677.0$	kg
m_{S}	Mass of the semitrailer	$25,323.0$	kg
I_T	Moment of inertia of the tractor	$4.61 \cdot 10^4$	$kg \cdot m^2$
I_S	Moment of inertia of the semitrailer	$4.52 \cdot 10^5$	$kg \cdot m^2$
a	Distance between points F and T	1.128	m
b	Distance between points T and R	2.422	m
c	Distance between points R and A	-0.31	m
d	Distance between points A and S	4.901	m
e	Distance between points S and M	2.399	m
n_{F}	Tires at the front axle	2	$-$
n_{R}	Tires at the rear axle	4	$-$
n_{M}	Tires at the semitrailer axle	8	$-$
μ	Friction coefficient	0.3	$-$

behavior of simple and articulated vehicles. This project is an ongoin work started at *Centro Universitário FEI* intended to develop open source packages with a fundamental and theoretical approach to the numerical simulation of vehicle systems. The package and the detailed documentation along with the theoretical foundation can be downloaded at *https://github.com/andresmendes/Vehicle-Dynamics-Lateral*.

The vehicle parameters of the simulation model represent a typical tractor semitrailer combination and are listed in Tab. 1. Thereby, the mass over each axle is given by $m_{\mathrm{F}} = 6,000.0\,kg$, $m_{\mathrm{R}} = 10,000.0\,kg$ and $m_{\mathrm{M}} = 17,000.0\,kg$, which correspond to the weight limits of Brazilian legislation for the number of tires used in each axle. The negative value of c indicates that the articulation point lies within the wheelbase of the tractor.

The tire model parameters represent a characteristic curve of a comercial truck tire and are listed in Tab. 2.

Table 2 – Articulated vehicle model - *magic formula* tire parameters.

Item	Description	Value	Unit
$\mathtt{a}_0$	Shape factor	1.003	$-$
$\mathtt{a}_1$	Load dependency of friction coefficient	2.014	$1/kN$
$\mathtt{a}_2$	friction coefficient level	710.501	$-$
$\mathtt{a}_3$	Maximum cornering stiffness	$5.226 \cdot 10^3$	N/deg
$\mathtt{a}_4$	Load at maximum cornering stiffness	78.877	kN
$\mathtt{a}_5$	Camber sensitivity of cornering stiffness	0.011	$1/deg$
$\mathtt{a}_6$	Load dependency of E	-0.005	$1/kN$
$\mathtt{a}_7$	E level	0.670	$-$

To illustrate the performance of the simulation model two cases are presented below where two different and arbitrary initial conditions are given to the system with no input. Hence, $\delta = 0\,rad$, $F_{x,\mathrm{F}} = 0N$, $F_{x,\mathrm{R}} = 0N$ and $F_{x,\mathrm{M}} = 0N$. The integration parameters can be found in Tab. 3 for both cases. For the first case $\alpha_{\mathrm{T},0} = 0.3\,rad$, $\dot{\psi}_0 = 0.25\,rad/s$ and $\dot{\phi}_0 = 0.25\,rad/s$ and for the second case $\alpha_{\mathrm{T},0} = 0.0\,rad$, $\dot{\psi}_0 = 0.4\,rad/s$ and $\dot{\phi}_0 = 0.4\,rad/s$. The simulation time is $12\,s$ and $15\,s$ for the first and second case, respectively. The remaining integration parameters are the same.

Table 3 – Articulated vehicle model - Integration parameters.

Item	Description	Value (Case 1)	Value (Case 2)	Unit
t	Simulation time	12	15	s
x_0	Initial longitudinal position	0.0	0.0	m
y_0	Initial transversal yaw angle	0.0	0.0	m
ψ_0	Initial yaw angle	0.0	0.0	rad
ϕ_0	Initial relative yaw angle	0.0	0.0	rad
$v_{\mathrm{T},0}$	Initial speed	20.0	20.0	m/s
$\alpha_{\mathrm{T},0}$	Initial vehicle side slip angle	0.3	0.0	rad
$\dot{\psi}_0$	Initial yaw rate	0.25	0.4	rad/s
$\dot{\phi}_0$	Initial relative yaw rate	0.25	0.4	rad/s

In Fig. 2 (a) and (b) the vehicle is plotted at different stages of the maneuver. This illustration is a specific graphic feature of the *Vehicle Dynamics - Lateral* package. The tractor is represented by the smallest rectangle and the semitrailer by the larger one. The trajectories of each axles are also shown.

In Fig. 2(a) the vehicle moves sideways and rotates. The relative yaw angle oscillates with decreasing amplitude and converge to zero. Finally, the vehicle travels in a straight line but in a different direction from the initial one. Figure 3(a) shows the CG acceleration signal for the first case maneuver. This behavior is considered favorable because there is no

Figure 2 – Successive frames of the articulated vehicle maneuver.

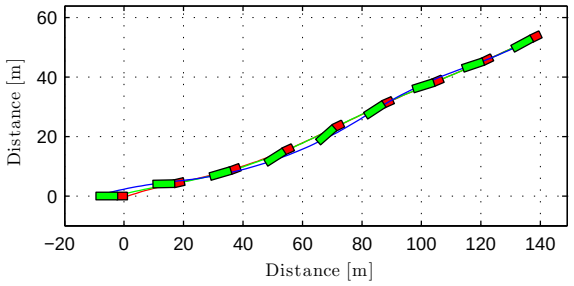

(a) Case 1. Without jackknifing (The first 8 s of the maneuver).

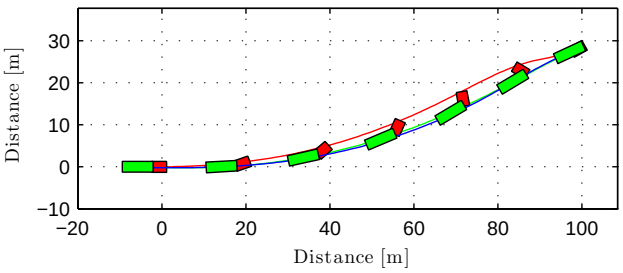

(b) Case 2. With jackknifing (The first 6 s of the maneuver).

jackknife event and the maximum lateral acceleration does not exceed the stipulated rollover threshold ($0.35\,g$).

Figure 2(b) shows the maneuver in which the lateral force of the tires are not able to prevent the excessive yaw rate of the tractor causing the jackknife. Again, Fig. 3(b) shows the CG acceleration signal for this maneuver. It is important to note that, in spite of the occurrence of jackknifing, the maximum lateral acceleration is maintained below the rollover threshold during the entire maneuver.

Figure 3 – Acceleration for both cases.

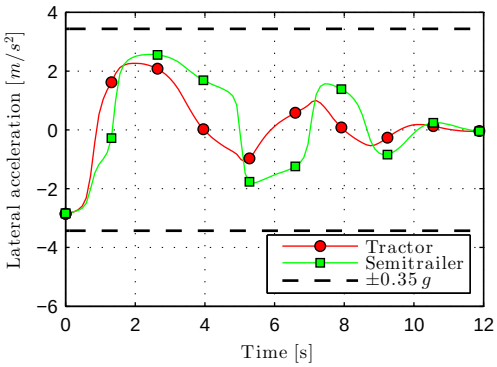

(a) Case 1. Without jackknifing

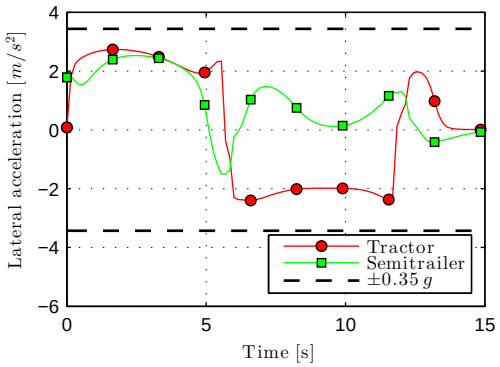

(b) Case 2. With jackknifing

RESULTS AND DISCUSSION

As discussed so far, the steady-state condition of the system with no input consists in the movement of the vehicle in a straight line with a specific final speed. However, not every final condition of the model is achieved without the occurance of instability events. If α_T converges, for instance, to $+\pi\,rad$ or $-\pi\,rad$ the vehicle travels in a straight line but it is evident that the tractor is moving backwards. Therefore, it is possible to trace the convergence region in a phase plane where all the initial conditions converge to the movement of the vehicle in a straight line without the occurrence of jackknife or rollover. Additionally, in the maneuver of interest the value of ϕ should not assume values greater than $90\,deg$ due to the constructive characteristics of the vehicle. Besides that, the initial relative yaw rate $\dot{\phi}_0$ gets the same value assigned to the initial condition $\dot{\psi}_0$ throughout the phase plane sweep. This feature ensures an initial relative rotation between the two units.

The phase plane used in this section is composed by the two most representative yaw-related states, α_T and $\dot{\psi}$. All other states and relevant quantities are monitored for assessing the initial conditions.

In Fig. 4, it is possible to observe the phase plane with three different convergence regions and several state orbits converging to three different fixed points. The central area in red indicates the initial conditions that converge to the final configuration of interest. In the upper region (green) the state α_T converges to $-\pi\,rad$. Similarly, in the lower region (blue) the state α_T converges to $\pi\,rad$. In all cases, the state $\dot{\psi}$ converges to zero indicating the dissipative characteristic of the system. In these adjacent regions the tractor completes the movement traveling backwards. The outermost regions at the top and bottom of the graphic enclose the initial conditions in which $|\alpha_T|$ converges to values greater than or equal to $2\pi\,rad$.

The phase plan was discretized vertically from point $\dot{\psi} = -1.395\,rad/s$ to the point $\dot{\psi} = 1.395\,rad/s$ in steps of $\Delta\dot{\psi} = 0.015\,rad/s$ and in the horizontal direction from the point $\alpha_T = -1.560\,rad$ to the point $\alpha_T = 1.560\,rad$ in steps of $\Delta\alpha_T = 0.015\,rad$. So, the phase plane grid has $39,083$ points. The system is integrated for each initial condition with

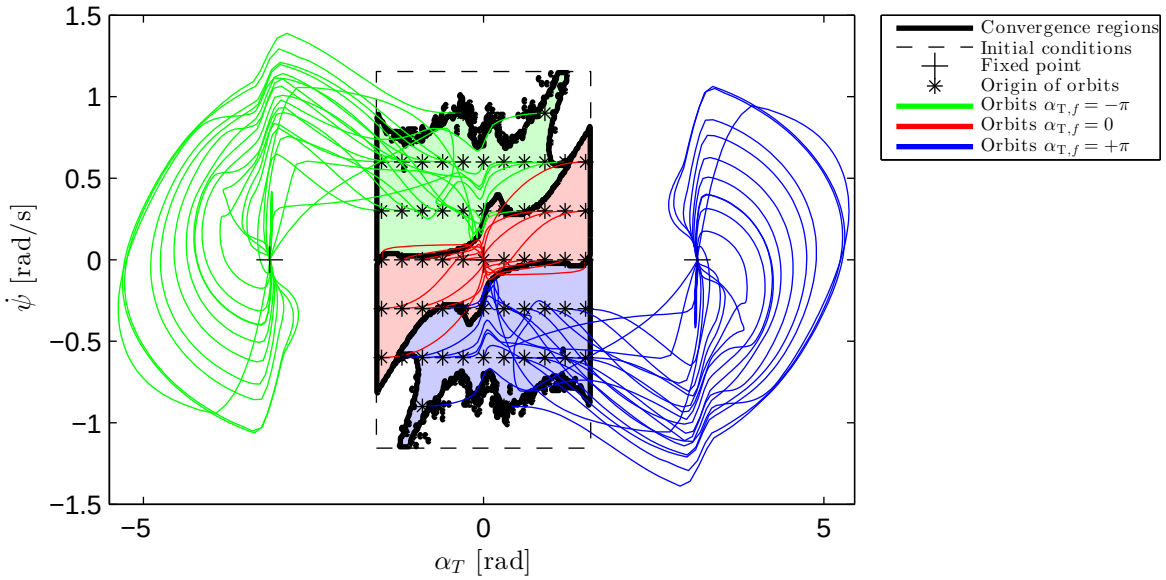

Figure 4 – Convergence regions and state orbits.

the vehicle data presented in Tab. 1. The integration time is $20\,s$ with resolution of $0.1\,s$. The configuration of the states to which the system converges is checked and the initial condition is marked appropriately. The maximum value of the relative yaw angle and the maximum values of the lateral acceleration of the two units are also checked. The lateral acceleration threshold is $0.35g$. If the system converges to the pair $(\alpha_{T,f} = 0, \dot{\psi}_f = 0)$ and the other criteria are also satisfied the initial condition is part of the region of interest. Otherwise it is assigned to one of the adjacent region.

Varying the CG velocity

In this section we investigate the variation of the convergence region according to the initial speed of the center of gravity of the tractor $v_{T,0}$. The vehicle parameters are the same as shown in Tab. 1 and the phase plane sweep is performed for each value of the initial speed. The discretization of the phase plane is made with the same resolution used in the previous section. The analyzed speed range goes from $v_{T,0} = 10\,m/s$ to $v_{T,0} = 30\,m/s$ in steps of $\Delta v_{T,0} = 2\,m/s$, totaling eleven initial speeds. Figure 5 shows the change in the convergence region as a function of the variation of the initial speed of the tractor in the phase plane.

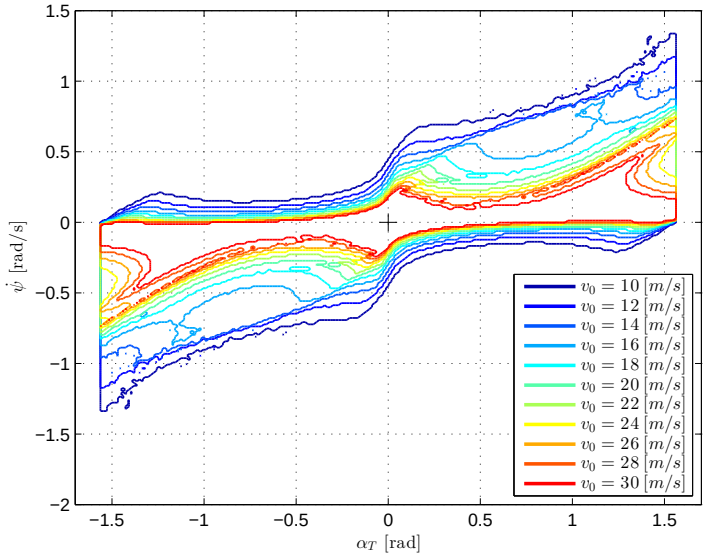

Figure 5 – Convergence region (2D) with varying CG velocity

The total area of the convergence region decreases with the increase of the initial speed of the tractor. For positive values of α_T (transversal component of the velocity vector $\mathbf{v}_T$ pointing to the left of the vehicle) the convergence region is, for all speeds, larger when the yaw rate is positive (vehicle turning counter-clockwise) than when the yaw rate is negative (vehicle turning clockwise). This implies that for $\alpha_T > 0$ a small negative initial yaw rate puts the system out of the

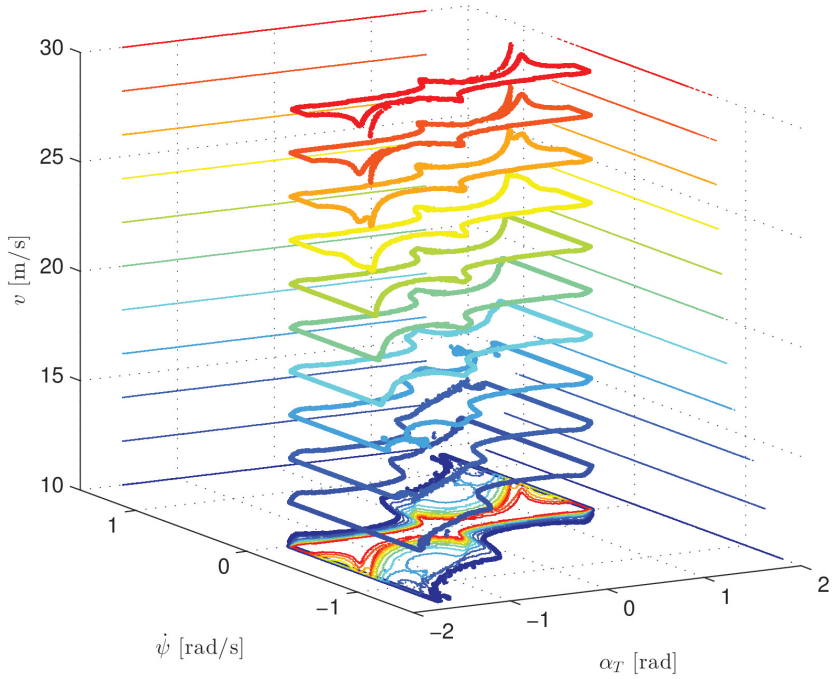

Figure 6 – Convergence region (3D) with varying CG velocity.

convergence region. However, the first quadrant region which is larger for smaller initial speeds, has its area significantly reduced as the initial speed increases. Meanwhile, in the fourth quadrant the displacement of the convergence region border is smaller. A similar analysis can be made for negative values α_T due to the anti-symmetry of the convergence region.

The illustration in three dimensions, the third axis being the initial velocity, is shown in Fig. 6. The curves of the regions are projected in the three perpendicular planes.

Varying the articulation point

This section shows the variation of the convergence region caused by different logitudinal positions of the articulation point. The values of the quantity that indicates the position of the articulation point in relation to the rear axle of the tractor range from $c = -0.5\,m$ to $c = +0.5\,m$ in steps of $\Delta c = 0.1\,m$, totaling eleven values. It is important to note that negative values of c indicate that the articulation point lies between the wheelbase of the tractor and positive values indicate that the articulation lies behind the rear axle of the tractor.

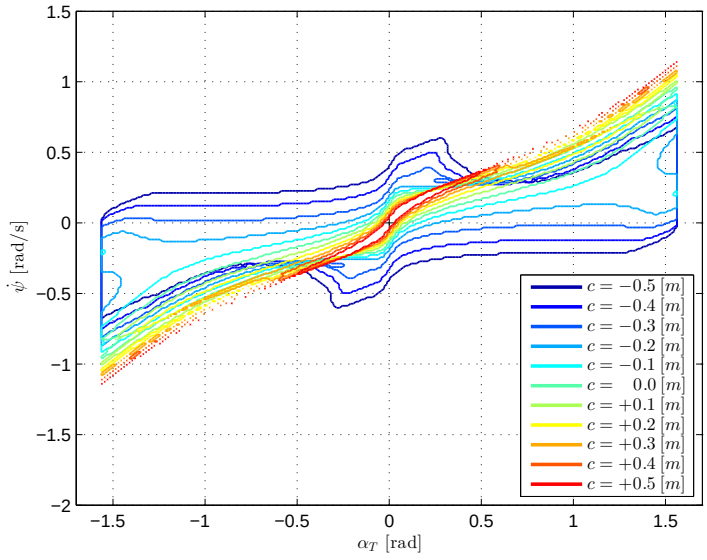

Figure 7 – Convergence region (2D) with varying articulation point.

The discretization of the phase plane ranges vertically from $\dot{\psi} = -1.14\,rad/s$ to $\dot{\psi} = +1.14\,rad/s$ in steps of $\Delta\dot{\psi} = 0.015\,rad/s$ and horizontally from $\alpha_T = -1.560\,rad$ to $\alpha_T = +1.560\,rad$ in steps of $\Delta\alpha_T = 0.015\,rad$. This resolution

forms a phase plane with 31,977 points. Figure 7 shows the variation of the convergence region in the phase plan for each value of c.

The region with the largest area in the phase plane has the articulation point at $c = -0.5\,m$ and as the value of c increases the total area decreases until the smallest area at $c = +0.5\,m$. Two different phenomenon can be observed with respect to the changes experienced by the region of convergence. The first is the narrowing of the region toward the state ψ, i.e. for a given state value of α_T the set of values of ψ contained in the convergence region decreases as the value of c increases. The second phenomenon is the rotation of the convergence region. The region, which for $c = -0.5\,m$ is approximately horizontal, rotates counter-clockwise and become diagonal when $c = +0.5\,m$. A consequence of these rotation is the increase of the range of ψ which can contain convergent initial conditions, despite the significant reduction of the total area of the region.

Moreover, as the quantity c increases you can check the fragmentation of the region into several smaller regions, although a larger central region of convergence is maintained. This effect may be due to the phase trajectory method which makes use of the discretization of the phase plane. However, it is also reasonable to assume that the system shows this kind of characteristic.

The variation in the convergence region is shown again in Fig. 8 with overlaid curves in three dimensions on a graphic in which the additional axis is given by c.

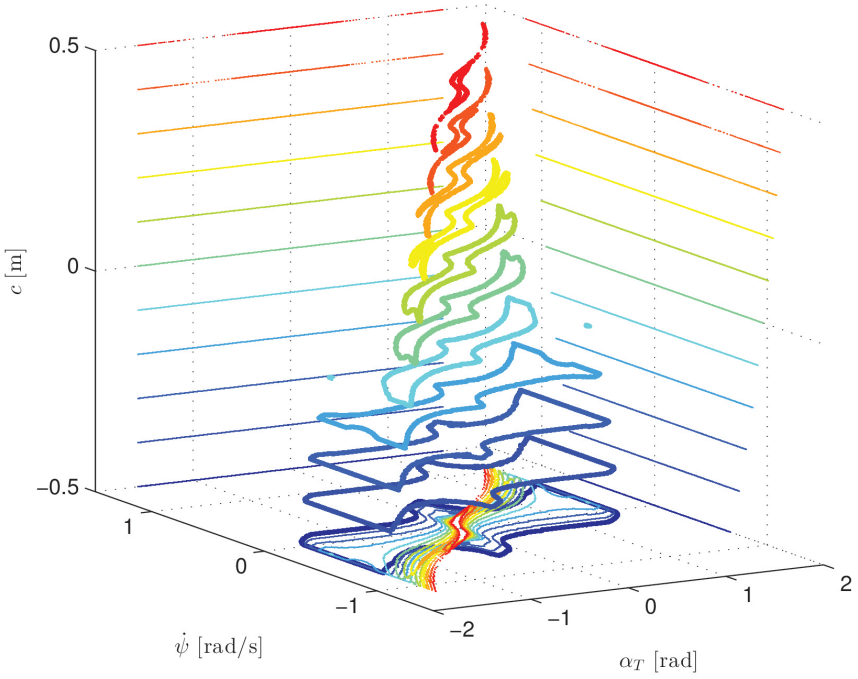

Figure 8 – Convergence region (3D) with varying articulation point.

CONCLUSION

The phase trajectory method allowed the estimation of a convergence region in the phase plane for an articulated vehicle composed by a tractor and a semitrailer. The integration of the system with a initial condition belonging to the interest convergent region produces a maneuver in which the vehicle ends up traveling in a straight line without the occurance of instability events such as jackknife and rollover. Furthermore, the variation of this convergence region is analysed as a function of the tractor speed and the position of the articulation point. In all cases it is possible to observe convergent initial conditions predominantly in the first and third quadrant of the phase plane. As the speed increases and the articulation point moves backwards the convergence region becomes smaller. Particularly, the variation of c produces the narrowing and rotation of the these region.

ACKNOWLEDGMENTS

These research was supported (master's scholarship) by the Brazilian research funding agency *Coordenação de Aperfeiçoamento de Pessoal de Nível Superior* (CAPES).

REFERENCES

Bakker, E.; Pacejka, H. B.; Lidner, L., "A new tire model with an application in vehicle dynamics studies", SAE paper, v. 890087, p. 101–113, 1989.

Ding, N.; Shi, X.; Zhang, Y.; Chen, W., “Analysis of bifurcation and stability for a tractor semi-trailer in planar motion”, Vehicle System Dynamics, Taylor & Francis, v. 52, n. 12, p. 1729–1751, 2014.

Ejzenberg, S., “Heavy vehicles and safety in the design of horizontal curves of roads and rapid transit routes”, Master’s Thesis — Universidade de São Paulo, São Paulo, 2009. (In Portuguese: Os veículos pesados e a segurança no projeto das curvas horizontais de rodovias e vias de trânsito rápido)

Ervin, R. D.; Nisonger, R. L.; Mallikarjunarao, C.; Gillespie, T. D., “The yaw stability of tractor-semitrailers during cornering”, The University of Michigan. Highway Safety Research Institute, 1979.

Fancher, P.; Winkler, C., “Directional performance issues in evaluation and design of articulated heavy vehicles”, Vehicle System Dynamics, Taylor & Francis, v. 45, n. 7-8, p. 607–647, 2007.

Hac, A.; Fulk, D.; Chen, H., “Stability and control considerations of vehicle-trailer combination”, SAE International Journal of Passenger Cars, SAE International, 2008.

Islam, M. M.; He, Y.; Zhu, S.; Wang, Q., “A comparative study of multi-trailer articulated heavy-vehicle models”, Journal of Automobile Engineering , v. 229, n. 9, p. 1200–1228, 2014.

Johnson, D.; Huston, J., “Nonlinear lateral stability analysis of road vehicles using Liapunov’s second method”, SAE Technical Paper, SAE International, 1984.

Luijten, M. F. J., “Lateral dynamic behaviour of articulated commercial vehicles”, Master’s Thesis — Technische Universiteit Eindhoven, 2010.

Maas, J., “Jackknife stability of a tractor semi-trailer combination”, Master’s Thesis — Technische Universiteit Eindhoven, 2007.

Mendes, A. S., “Yaw stability analysis of articulated vehicles”, Master’s Thesis — Centro Universitário FEI, 2016. (In Portuguese: Análise de estabilidade em guinada de veículos articulados)

Mendes, A. S.; Meneghetti, D. R., “Vehicle Dynamics - Lateral”, 2015. Available in: *https://github.com/andresmendes/Vehicle-Dynamics-Lateral*

Pacejka, H. B. Tyre and vehicle dynamics. Oxford: Elsevier, 2006.

Pauwelussen, J. P., “Excessive yaw behaviour of commercial vehicles, a fundamental approach”, In: International Technical Conference on the Enhanced Safety of Vehicles, 17, 2001, Enhanced Safety of Vehicles (ESV), 2001.

Sadri, S.; Wu, C. Q., “Stability analysis of a nonlinear vehicle model in plane motion using the concept of Lyapunov exponents”, Vehicle System Dynamics, Taylor & Francis, v. 51, n. 6, p. 906–924, 2013.

Samsundar, J.; Huston, J. C., “Estimating lateral stability region of a nonlinear 2 degree-of-freedom vehicle”, SAE Technical Paper, 1998.

Stotsky, A.; Hu, X., “Stability analysis of robustly decoupled car steering system with nonlinear tire model”, In: Conference on Decision and Control, 36, 1997. Decision and Control. IEEE, 1997.

Sun, T.; He, Y., “Phase-Plane Analysis for Evaluating the Lateral Stability of Articulated Vehicles”, SAE Technical Paper, 2015.

Wideberg, J.; Dahlberg, E.; Svensson, M., “A comparative study of legislation and stability measures of heavy articulated vehicles in different regions”, International Journal of Heavy Vehicle Systems, Inderscience, v. 16, n. 3, p. 354–361, 2009.

Winkler, C. B.; Ervin, R., “Rollover of heavy commercial vehicles”, The University of Michigan. Transportation Research Institute, 1999.

Yan, Y.-g.; Xu, H.-g.; Liu, H.-f., “Estimating Vehicle Stability Region Based on Energy Function”, Discrete Dynamics in Nature and Society, Hindawi, v. 2015, p. 1–7, 2015.

Yin, G. D.; Jin, X. J.; Qing, Z. Y.; Bian, C. T., “Lateral stability region conservativeness estimation and torque distribution for FWIA electric vehicle steering”, Science China Technological Sciences, Science China Press, v. 58, n. 4, p. 669–676, 2015.

RESPONSIBILITY NOTICE

The authors are the only responsible for the material included in this paper.